ADVANCED MATERIALS INTERFACES
Open Access
www.advmatinterfaces.de

Advanced DNA–Gold Biointerface for PCR-Free Molecular Detection of *Leishmania infantum*

Paolo Calorenni, Giovanni Bella, Marco Sebastiano Nicolò, Emanuele Luigi Sciuto, Maria Vittoria Balli, Giovanni Valenti, Tommaso Gritti, Stefania Varani, Luca Prodi, and Sabrina Conoci*

PCR-free approaches are the most promising technologies for molecular point-of-care (PoC). In this context, the detection of not amplified genetic targets through electro-optical transduction is successfully investigated. While PCR-free approaches are widely studied, there are only a few studies investigating the factors that modulate both the kinetics and the effectiveness of target capture. Among these, the probes grafting density and the isoelectric properties of the biointerface are crucial since they conditionate the charge field around biomolecules during and after the target recognition. In this work, an experimental and theoretical study of a gold biointerface functionalized with oligonucleotide probes is presented for the direct detection by cooperative hybridization of the kinetoplast (k)DNA of *Leishmania infantum*(LI). The biointerface is characterized by surface free energy (SFE) analysis and contact angle (CA) to investigate the grafting of probes and the surface isoelectric properties upon the duplex formation with the genetic target. Experimental data are compared with a theoretical model, based on the prediction of adsorption energies, which effectively reflects the charge profile of the functionalized surface. Lastly, the biointerface is characterized by electrochemical impedance spectroscopy (EIS) and the sensing performances assess in the frame of its suitability for PoC applications.

1. Introduction

The detection of nucleic acid (NAs) is extremely important for several biomedical applications, including gene expression analysis, diagnosis of infectious diseases and screening of genetic syndromes; its technological evolution is also paving the basis for personalized medicine.

The new frontier of DNA analysis is moving toward PCR-free approaches based directly identifying not amplified genetic targets by a surface-mediated hybridization with solid-state immobilized single-stranded (ss) DNA oligonucleotide probes.[1] This approach provides relevant advantages with respect to the traditional procedures for DNA identification and quantification since it excludes PCR amplification, thus leading to faster, cheaper, and simpler lab-free analyses.[2–5] Such improvements led to the introduction of innovative genetic point-of-care (PoC) technologies, where DNA detection is perfectly embedded on functionalized surfaces integrated in portable, accurate and robust sensing platforms that allow to decentralize the entire molecular analysis.[6–8]

Several studies were carried out on the implementation of the sensing system architecture and the PCR-free strategy detection, which is mainly based on a cooperative hybridization mechanism.[9] However, to date, only a few of them focus on the factors that modulate both the detection performance and the kinetics of capture probes towards not amplified genetic targets in a sensing surface.

P. Calorenni, G. Bella, M. S. Nicolò, E. L. Sciuto, S. Conoci
Department of Chemical, Biological
Pharmaceutical and Environmental Sciences
University of Messina
Viale Ferdinando Stagno d'Alcontres 31, Messina 98166, Italy
E-mail: emanueleluigi.sciuto@unime.it

The ORCID identification number(s) for the author(s) of this article can be found under https://doi.org/10.1002/admi.202400642

DOI: 10.1002/admi.202400642

M. V. Balli, G. Valenti, L. Prodi, S. Conoci
Department of Chemistry "Giacomo Ciamician,"
University of Bologna
Via Francesco Selmi 2, Bologna 40126, Italy
T. Gritti, S. Varani
Department of Medical and Surgical Sciences
University of Bologna
Via Massarenti 9, Bologna 40138, Italy
S. Conoci
URT LAB SENS DSFTM CNR Messina
Viale Ferdinando Stagno d'Alcontres 31, Messina 98166, Italy

The grafting density of immobilized probes and their relative isoelectric features can affect both the efficiency and kinetics of duplex DNA formation in the genetic target capture mechanism.[10] Indeed, the probes have a strong effect on the hybridization with DNA, which, as strong negatively charged polyelectrolyte, can cause repulsive electrostatic interactions between the helical motifs involved in the binding.[11,12] Gong and Levicky indicated that higher grafting density does not always lead increased double strand (ds) DNA pairing, as under certain conditions, higher grafting density can strongly suppress the hybridization.[13] The idea that the grafting of probes can directly influence the efficiency of surface-mediated hybridization is supported by other evidence showing a correlation between grafting density and entropic forces and how this interaction plays an important role in the conformation of hybridized DNA immobilized on the surface.[14–17] On the other hand, the isoelectric characteristics of NAs, as a function of their basic and acidic residues and the combinations of their pK values,[18] can also influence the hybridization process. In their reaction environment, NAs assume specific spatial configurations that are compatible with their thermodynamic equilibrium. This structural organization is determined by the primary structure and ionogenic groups within the DNA chains (of both probe and genetic target), which make these macromolecules are susceptible to pH changes consistent with their isoelectric properties. Thus, the reaction environment can modulate not only the wettability of the functionalized sensing surface, but also the formation of the probe-target duplex, as the electrostatic interactions of the DNA chains must be energy-minimized to favor the occurrence of hybridization. The use of isoelectric data as a means of characterization is a fairly new approach and was first introduced by Sherbet and Lakshmi[19,20] in the analysis of cell surfaces, which were considered analogous to multivalent ions, and in the investigation of some secondary structures of NAs.[21] According to this evidence, the investigation of surface chemical properties, in terms of wettability and isoelectric profile of immobilized and hybridized solid-state DNAs becomes crucial for the design of a new genetic PoC system.

In this context, recent developments in theoretical modeling, specifically the density functional theory (DFT), have enabled quantum theory and molecular simulation methods to offer effective computational tools for studying molecular interfaces.[22–24] In this landscape, in the current decade investigation of the adsorption properties (such as hydrophobicity, hydrophilicity, wettability) received deep attention, with a vigorous rise of the DFT studies concerning water/metal interface.[25,26] However, computational analyses of the surface characteristics of molecular biosensor platforms based on the capture of genetic material are still in their infancy.

In this work, the surface chemical properties of a DNA-functionalized gold biointerface before and after the hybridization with a not amplified target have been characterized by SFE and CA analysis. The gold substrate has been prepared by grafting a self-assembled monolayer (SAM) of 5′ thiol-modified oligonucleotide probes selective towards the molecular detection of *Leishmania infantum*, an hemoflagellate protozoan (family Trypanosomatidae, order Kinetoplastida, genus *Leishmania*) that causes visceral leishmaniasis, a potentially lethal disease.[27] This unicellular eukaryotic pathogen contains multiple copies (approximately 0.5–1 × 10^4 copies per parasite's cell) of the 0.8–2 Kbp minicircular kDNA, which is located inside the mitochondria and regulates the expression of the entire *Leishmania* genome.[28] When causing visceral leishmaniasis, the parasite replicates in cells of the reticuloendothelial system and can be detected by real-time PCR assays in peripheral blood and bone marrow aspirates.[29] PCR-based methods represent a relatively recent development in clinical *Leishmania* diagnostics that overcomes the limitations of previous detection methods in terms of test sensitivity and specificity, allowing the employment of peripheral blood as a clinical specimen and avoiding invasive procedures to obtain bone marrow samples. The interface wettability was studied after the probes anchoring and the cooperative hybridization of probes with the kDNA and the isoelectric properties were also evaluated through CA at different pHs. A theoretical modelling has also been implemented to correlate the CA data with the probe molecular structure as a function of its nucleotide chemical composition.

The kDNA detection performances of the DNA-functionalized biointerface were also tested by EIS as a first trial of future PoC biosensing applications.

2. Results and Discussion

The biointerface is a crucial component for biosensor since it strongly affects the bio-recognition processes and, as a consequence, the performance of the sensing. This is particularly relevant for PCR-free detection where the starting target concentration is very low.[30] Therefore, CA characterization (see "Background" in Figure S1 of Supporting Information) of the DNA–gold functionalized interface has been performed in order to investigate the changes of surface charges occurring in the interfaces upon the bio derivatization and molecular recognition.[31–33]

LI1 and LI2 probes were properly designed to recognize an inner region of the *L. infantum* kDNA. The probes sequences were selected considering both dimension and degree of conservation of the complementary regions inside the genetic target. Moreover, it was guaranteed an optimal sequence composition, with a guanine-cytosine content percentage below 50%, a good melting temperature, between 50 °C and 70 °C, and a proper chemical derivatization, with alkyl thiol group added at the 5′ end of the sequence for the SAM formation on gold.

The CA characterization of step-by-step functionalized DNA–gold biointerface is shown in **Figure 1**. Figure 1a reports the scheme of the chemical steps used for the Au surface functionalization and not amplified genetic target recognition. The corresponding CA measures are plotted in Figure 1b. Data highlight a marked increase of wettability after the Au cleaning step, passing from 80.76° ± 1.03° to 51.93° ± 3.34° of CA, which could be related to the formation of the thin hydroxyl layer on the gold surface. After the grafting of oligonucleotide probes the wettability increased again, as proved by the relevant decrease in CA of ≈40° reported in the figure. These changes were due to the addition of charges to the gold surface, brought by the hydroxyl, amino and phosphate groups of the oligonucleotide chains that led to a higher number of electrostatic interactions between the water drop and the surface.

The functionalized biointerface was, then, treated with 10^7 copies per μL of the kDNA target. The cooperative hybridization

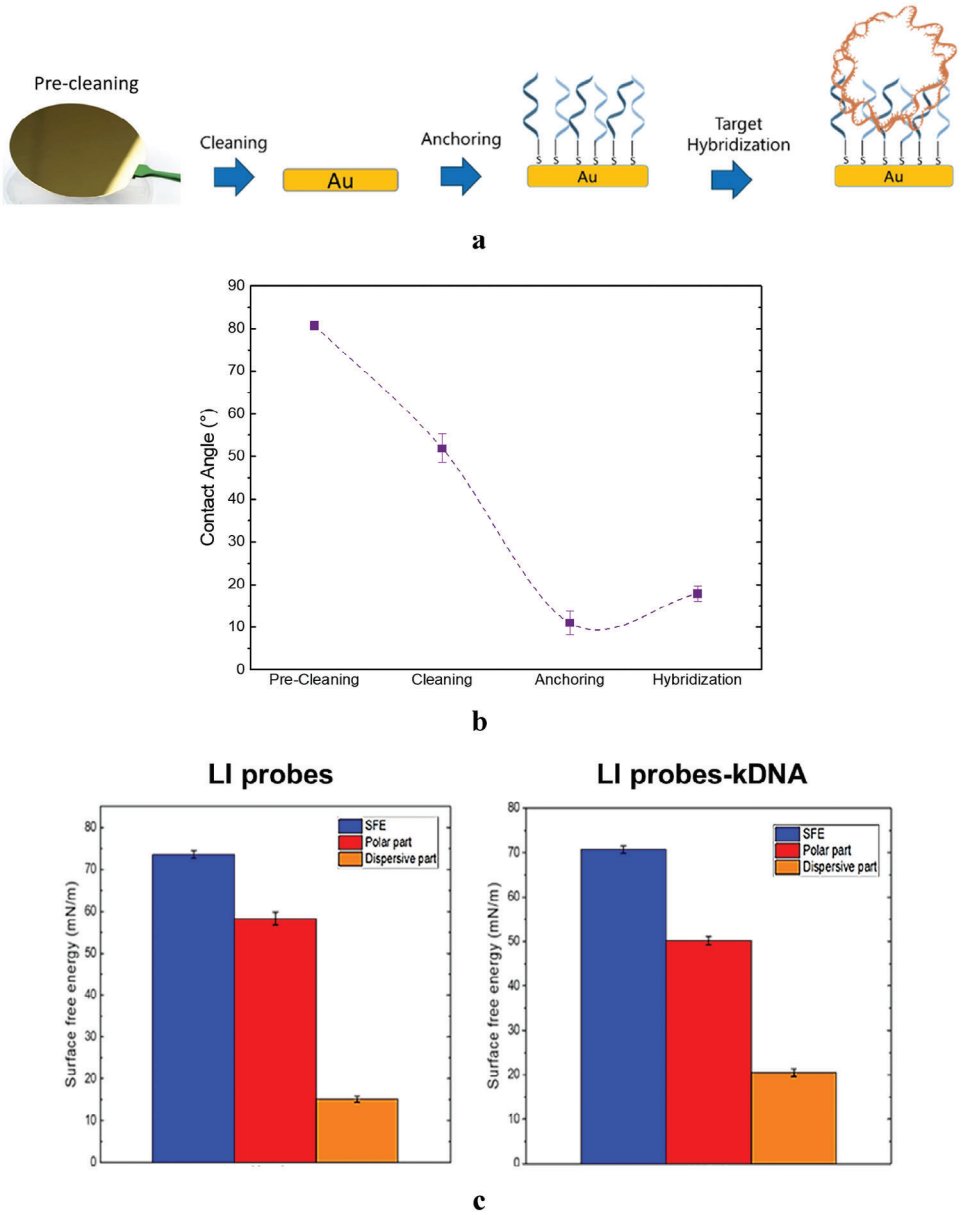

Figure 1. a) Gold substrate chemical functionalization with LI1/2 probes (in blue) and kDNA target (in orange); b) step-by-step CA characterization of functionalized biointerface; c) SFE analysis on DNA–gold functionalized biointerface before (LI probes) and after (LI probes-kDNA) the kDNA hybridization, with detail of total SFE (blue), polar component (red) and dispersive component (orange) values.

was performed according to a previous work of PCR-free detection of Hepatitis-B Virus genome.[2] The advantage of using such hybridization mechanism is that the two use-case probes simultaneously recognize and hybridize two close regions of the same kDNA molecule, with a recognition sequence gap of ≈90 bp that minimizes the steric hindrance[34] in the probe-target interaction and increases both yield and stability of the DNA capture. As shown in Figure 1b, CA analysis after the step of kDNA hybridization proved that the biointerface almost maintained high hydrophilicity and wettability, reporting a value of 16.58 ± 1.13°. This slight increase in CA value, compared to that measured on biointerface with probes only, is due to molecular recognition.[35] Indeed, the binding between oligo and target chains causes a partial shielding of the charges exposed by the functional groups of single-strand probes affecting the biointerface polarity.

To test our hypotheses, an SFE analysis in OWRK method (see "Background" in Figure S1 of Supporting Information) was performed on the DNA–gold biointerface before and after the kDNA hybridization. The results for the biointerface exposing probes only, described in Figure 1c-LI probes, reported a high SFE value of 73.60° ± 0.90 mN m^{-1} with a predominant polar part at 58.27 ± 1.55 mN m^{-1}, due to the addition of oligonucleotides charges. The analysis after the kDNA hybridization, in Figure 1c-LI probes-kDNA, showed an SFE value of 70.66 ± 0.80 mN m^{-1} that proved the surface wettability was kept after the cooperative hybridization. However, a lower value of the polar part at

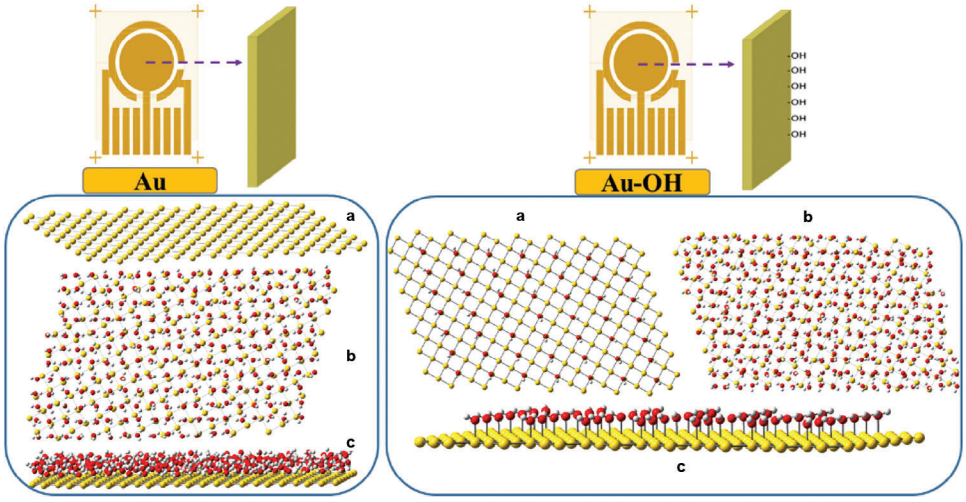

Figure 2. a) DFT-optimized pure gold slab. b,c) DFT-optimized water-gold system with frontal and lateral view, respectively. Right: a,c) DFT-optimized hydroxylated-gold support with frontal and lateral view, respectively. b) DFT-optimized water/gold-OH platform. It must be noted that for an easier visualization only a portion of the whole system is graphically reported.

50.17 ± 1.03 mN m^{-1} was also observed, clearly proving the formation of the double helix and the charges shielding effect as a consequence of probe-target hybridization.

To gain insight into the most favored oligo probe conformation at the interface, we performed theoretical research to computationally predict the wettability profile along the three main steps of the gold electrode functionalization process schemed in Figure 1a: pre-cleaning (Au, pure gold electrode), cleaning (Au-OH, hydroxylated gold electrode), and anchoring (Au-probes, probes-functionalized electrode). We introduced a computational workflow that implicates an accurate exploration of the ground state potential energy surfaces of the three mentioned systems to retrieve the thermodynamic parameters necessary to calculate the adsorption energy. This physical quantity was privileged to get a direct comparison between theoretical and experimental surface wettability measurements. **Figure 2** shows the DFT optimization of the first and the second step (pure gold and cleaned gold) in which the water molecules assumed a preferential conformation to positively interact with gold atoms and with the hydroxyl polarized groups on the metal layer, respectively.

Before starting with the assembled systems (third step, anchoring), the modelling of the isolated oligonucleotide probes (in solvent phase, water) selected for targeting the kDNA of LI was accurately performed (**Figure 3a**).

From the above-reported data, it emerges that energy minima (LI1, LI2) show a peculiar helical motif; additionally, it is possible to observe that in both optimized structures the hexyl thiol scaffold (linked to the 5′ pendant) realizes a precise intramolecular hydrogen bonding pattern. In particular, it is possible to observe a single hydrogen bond between the polarized hydrogen of the

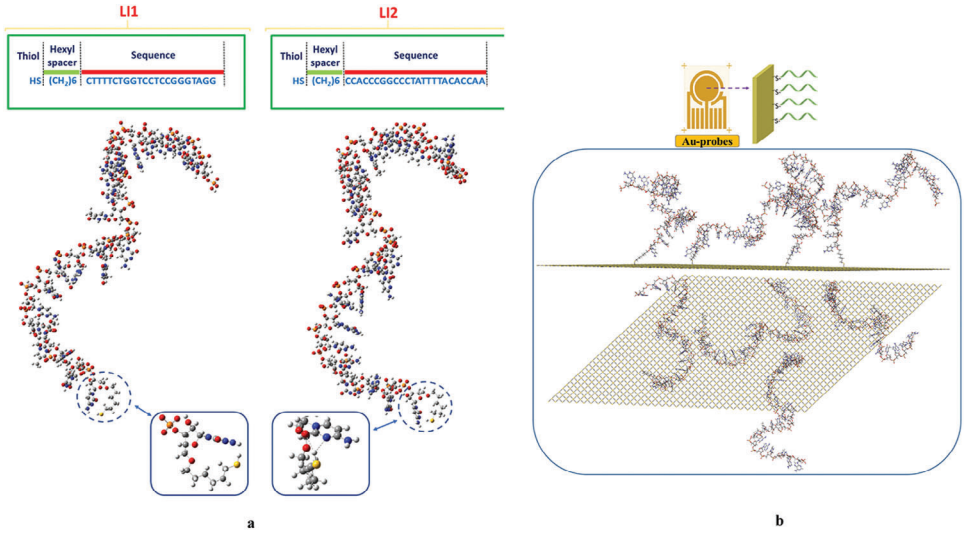

Figure 3. a) Optimized structures of LI1 and LI2 in water phase. The enlarged visions are referred to the intramolecular hydrogen bonding patterns. b) Optimized systems formed by LI1 and LI2 (4 probes) anchored to the gold surface. (Top) lateral view, (bottom) frontal view.

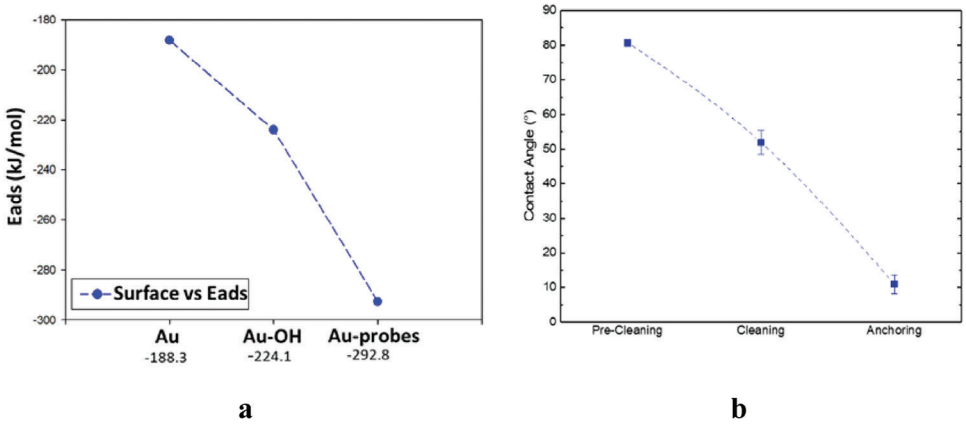

Figure 4. a) Calculated adsorption energies plot. b) Experimental contact angles graph.

thiol arm and the endocyclic nitrogen of the first base (cytosine) for LI1 (2.7Å), and a bifurcated network which involves a double hydrogen bond between the thiolic proton with the endocyclic nitrogen and with the exocyclic oxygen of the cytosine for LI2 (2.36 and 2.44 Å, respectively).

LI1 and LI2 were covalently bonded to the gold surface to obtain the final model (third step), as cropped up from both lateral and frontal views (Figure 3b), the relaxed system rearranges the probes to minimize the electrostatic repulsion but maintaining their helical shapes.

Once the three systems were quantum mechanically investigated, it was possible to collect their calculated thermodynamic parameters. In this context, the wettability of the H_2O molecules on the gold-functionalized surfaces can be expressed in terms of the adsorption energy, which resulted negative because of its exothermic behavior. Briefly, the lower the value, the stronger the adsorption hence the more stable the adsorption, the higher the wettability, and vice versa. The adsorption energy (E_{ads}) was computed as follows:

$$E_{ads} = E_{s/w} - E_s - E_w \quad (1)$$

where E_{ads} (kJ mol^{-1}) is the adsorption energy of the H_2O molecules on the surface of the gold functionalized platforms, $E_{s/w}$ is the total energy of the stabilized system after adsorbing water molecules on the surface (kJ mol^{-1}), E_s is the energy of the gold functionalized slab before adsorption (kJ mol^{-1}) and E_w is the energy of the water molecules before adsorption.

As reported in **Figure 4**, the theoretical graph of the adsorption energies (**4a**) and the experimental graph of contact angle data (**4b**) have the same trend moving from the more hydrophobic gold surface to the more hydrophilic probes-gold platform. Therefore, the wettability increases when moving from the pure gold to oligonucleotides-gold complex, evidencing how the more polar interface guaranteed by the oligonucleotide probes offers a very large number of hydrogen bonding sites (phosphate groups and the sequence of nucleobases) to accommodate the water molecules.

To further investigate the biointerface properties, we performed a CA study at various pH. The isoelectric properties and PZC of LI probes and LI probes-target (kDNA) biointerfaces have been analyzed through CA measurements at various pHs and results are reported in **Figure 5**. Actually, in the aqueous environment of the studied DNA–gold biointerfaces the equilibrium can be easily altered by changing the pH and the surface hydrophilicity[36] since the anchored biomolecules can be both positively and/or negatively charged with respect to their isoelectric properties and the point of zero charge (PZC).[37–39]

CA measured on the biointerface modified with LI probes only, Figure 5a, reached a maximum of 41.24° ± 2.43° at pH 5, considered as a possible PZC value, and decreased at other pHs. This trend could be explained as the consequence of the ionization of DNA amino, hydroxyl and phosphate groups when the pH is away from their PZC causing the increase of biointerface hydrophilicity and surface wettability.

In the case of biointerface with LI probes and kDNA, Figure 5b, the average contact angles highlighted a maximum of 32.47° ± 1.25° around pH 6 and, again, decreased at pHs that were different from the PZC. A slight increase, however, was observed also at pH 2, probably, since the kDNA molecule at that pH tends to denature and alter its isoelectric profile.

The final part of our study addressed the PCR-free sensing ability of our biointerface to test its suitability for further application in PoC molecular devices. More specifically, electrochemical impedance spectroscopy (EIS) experiments were carried out to detect non-amplified kDNA of LI. Three golden working electrodes were prepared with LI probes and kDNA target according to the protocol schemed in Figure S7 (Supporting Information) and results of the EIS tests after their functionalization have been reported in the Nyquist plots of **Figure 6**, while the specifications of measured resistance and capacitance values are resumed in **Table 1**.

As reported, the low charge electron transfer resistance at 132 Ω measured in the case of the bare gold electrode (black line in Figure 6) increased to 1417 Ω after the anchoring of LI probes (red line), as a consequence of the hindrance of the oligo probes and the electrostatic repulsions introduced between the negatively charged oligo and the analyte.[40]

Subsequently, the addition of the thiol passivator (blue line) to block the uncovered sites of the electrode surface caused a further increase in the resistance to the transfer of low-charge electrons to 3953 Ω. This enhancement was probably due to the

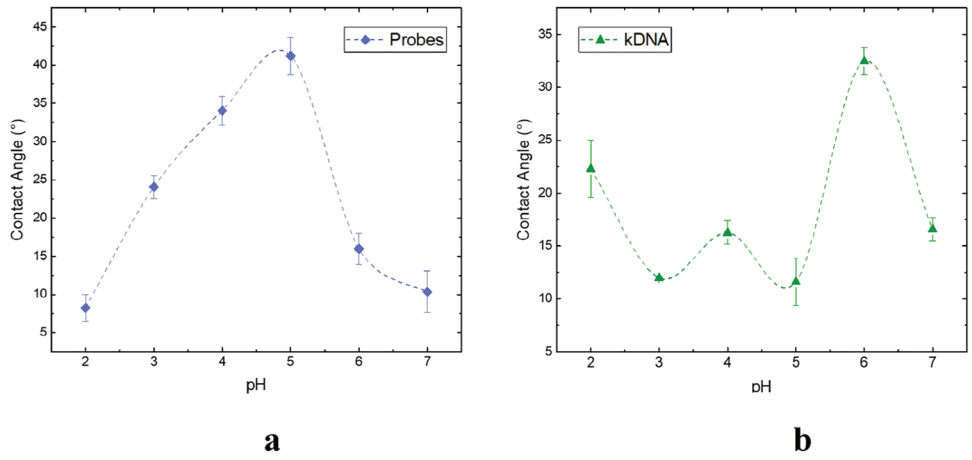

Figure 5. CA analysis of LI probes a) and LI probes-kDNA biointerface b) at various pHs.

blocking of sites free from the probes that limit the current in the redox reaction affecting also the EDL (see Figure S1 of Supporting Information) that retains more easily stationary charges between the passivator layer and the electrolytic solution.[41] The EIS performed on the electrodes after the hybridization with 10^7 copies per µL of kDNA (green line) revealed a marked increase of the resistance values above 11 kΩ as a consequence of the ds-DNA molecules capture and the increase of the dimensions of the EDL formed onto the electrode surface. The most significant difference between the reported electrodes occurs after the kDNA hybridization step, since the semicircular diameter markedly increases upon target addition. Moreover, the PCR-free sensing is selective and strictly dependent on the presence of the probes array as proved by the additional analyses performed on the Au electrode functionalized with probes after the addition of an unspecific (US) genome and the Au electrode treated with kDNA in absence of probes, reported in Figure S8a,b (Supporting Information), respectively. Thus, the electrochemical data suggest that all the steps leading up to the functionalization of the gold surface are functioning correctly. These data highlight the radical innovation brought by this method compared to the standard surface probe-target recognition methodologies based on the microarray that need a PCR amplification of the target before recognition.[42–45]

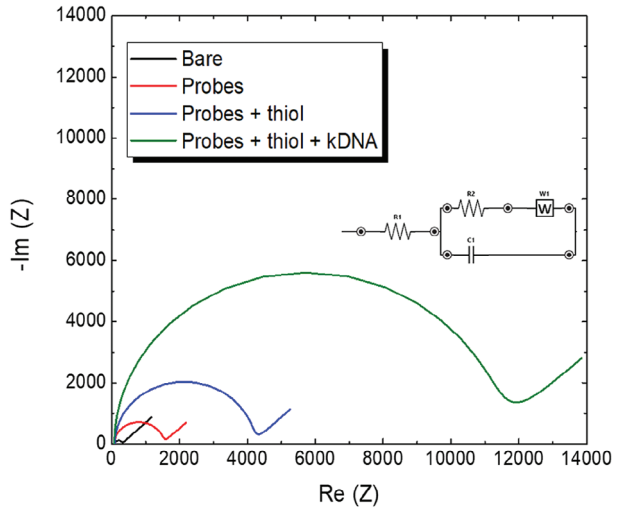

Figure 6. EIS experimental results of DNA-functionalized gold electrodes: Nyquist plot obtained bare (black line) and functionalized electrode by grafting of LI probes (red line), thiol passivator (blue line) and upon the hybridization with 10^7 copies per µL of kDNA (green line). All EIS measurements have been performed in the 0.1 Hz–100 kHz frequency range, thus it has been chosen to maintain fixed the current interval (1 mA). Open circuit potential (*E*ocp) fixed at 0.230 V for all the measurement time. Inserts: equivalent circuit for data fitting.

3. Conclusions

An experimental and theoretical investigation of the chemical-physical properties of gold biointerface functionalized with short oligonucleotide probes for the recognition of parasitic not amplified kDNA by direct cooperative hybridization has been proposed. The CA and SFE analysis of the gold surface after each step of functionalization reported an increase of surface wettability after the probes grafting and the target hybridization as a function of the hydroxyl, amino and phosphate groups addition brought by DNA chains causing the increase of electrostatic interactions between the drop and the surface. These variations in wettability confirmed the proper probes molecular layer anchoring for the effectiveness of PCR-free detection of kDNA through cooperative hybridization.

The theoretical workflow confirmed the wettability experimental data pointing out how the chemically different interfaces offer a variable number of sites for hydrogen bonding, which strongly affects the hydrophobicity/hydrophilicity of the whole system.

Furthermore, surface charge properties of the DNA–gold biointerface were studied by evaluating the variations in surface wettability at different acid pH values revealing a PZC at pH 5 for the LI probes and pH 6 for the kDNA. These results confirmed that when the pH is sufficiently far from the PZC, by modifying the ionic strength, it is possible to transform a surface with a highly hydrophilic character to a less hydrophilic one. Moreover, a greater slope of the CA versus pH curves was observed as the

Table 1. Resistance (*R*2) and capacitance (*C*1) comparison of functionalized electrodes.

Electrode	*R*2 [Ω]	*C*1 [μF cm^{-2}]
Bare	132	2.98
Probe	1417	39.56
Thiol	3953	49.68
Probe+kDNA	11 500	88.2

ionic strength increased, probably as a consequence of a reduction of the EDL thickness that influenced the surface wettability.

Lastly, the EIS analysis reported that the DNA–gold biointerface works properly for the recognition of *Leishmania infantum*. The marked increase of surface electrode resistance measured after the kDNA hybridization proved the biointerface ability to recognize the kDNA and its suitability for future applications in PoC diagnostic technologies.

4. Experimental Section

Chemicals: Ammonium hydroxide solution (NH_4OH) ACS reagent, 28.0-30.0%, NH_3 basis, hydrogen peroxide (H_2O_2) solution 30% (w/w) in H_2O, contains stabilizer, 0.01 M phosphate buffered saline (PBS) solution at pH 7.4, ultraPure water, 0.2 M phosphate buffer at pH 6.01, 0.2 M acetic acid/acetate buffers at pH 5.05, 4.01 and 3.7, and 0.01 M hydrochloric acid at pH 2, sulfuric acid (H_2SO_4) 0.5 M, potassium hexacyanoferrate $[Fe(CN)_6]^{3-/4-}$ (ratio 1:1) 5.0×10^{-3} M, 6-mercapto-1-hexanol ($C_6H_{14}OS$) and ethanol (C_2H_6O) 100% were purchased from Merck. All chemicals were used without further purification.

Oligonucleotide Probes and Genetic Target: The use-case probes were thiol-modified oligonucleotides designed according to Mary et al.[46] and selected for the recognition of LI kDNA because of their high sensitivity and specificity when used as primers for real-time PCR assay as well as adequate distance between the probes.[47] The LI1 and LI2 probes were HS-(CH2)6-CTTTTCTGGTCCTCCGGGTAGG and HS-(CH2)6-CCACCCGGCCCTATTTTACACCAA, respectively. Both probes were purchased from MetaBion International AG (Planegg, Germany). The hexyl fragment at 5′ end was added as a spacer for a proper orientation of probes once grafted on the electrode surface, while the thiol group allowed the thiol-gold complex and the self-assembled monolayer (SAM) formation. Probes target the conserved region of the kDNA minicircle molecules, a part of *Leishmania* spp. entire genomic DNA (gDNA).[28] The distance between the two internal ends is 94 base pairs (bp) when aligned against LI kDNA sequence (Accession number Z35273.1). gDNA of LI was obtained from promastigote cultures of the LI reference strain JPCM5 (MCAN/ES/98/LLM-877); parasites were harvested for DNA extraction at a concentration of 10^9 parasites mL^{-1}, as estimated by Bürker Chamber cell count with a ×200 objective under standard light microscopy. DNA extraction was performed by using the DNeasy Blood & Tissue kit (Qiagen, Hilden, Germany) and a semi-quantitative real-time PCR was carried out on the eluate to detect the target kDNA and to confirm the parasite concentration;[48] primers for the real-time PCR had the same nucleotide sequence as the use-case probes. As the number of minicircles varies within *Leishmania* species and strains,[46] we arbitrarily estimated 1×10^4 copies of minicircles per parasite's cell; the extracted DNA (from 10^9 parasites mL^{-1}) would contain 10^{10} kDNA copies mL^{-1}.

Gold Substrate for Biointerface Preparation: The gold substrate used for the DNA functionalization was a 0.55 cm × 1 cm gold-sputtered silicon substrate. The substrate was functionalized with LI probes and kDNA target according to the following chemical protocol. First, it was carried out a step of surface cleaning that has been deeply optimized to find the best compromise between dust and unspecific organic dendrites removal and surface gold layer preservation. The gold substrate was placed inside a Teflon container and, initially, rinsed 19 times with distilled water. Subsequently, a basic piranha solution (H_2O_2:NH_3:H_2O = 1:1:4) was spotted at 70 °C for 2 min to completely clean the surface. At the end of the process, the substrate was rinsed abundantly with ultrapure water and fluxed with nitrogen. Subsequently, the substrate was incubated with a 10×10^{-6} M solution of thiol-modified probes, suspended in PBS 0.01×10^{-3} M at pH = 7.4, at 25 °C for 4 h with 40 rpm of stirring.

This condition was required to allow the probes to be efficiently dispersed and favor the thiol-gold complex formation in a SAM configuration. The SAM enabled the probes to be exposed in the right orientation for the sensing interaction with the genetic target. Then, a washing step with PBS removed the unbound probes from the surface. For the not amplified genetic target hybridization, kDNA was directly used at a final concentration of 10^7 copies per μL in PBS at pH 5.5, prepared by diluting the 10^{10} copies per μL stock solution. The final gold surface functionalized with LI1/LI2 probes was dipped in kDNA solution at 50 °C for 3.5 h. Then, the unbound kDNA was washed away from the surface by PBS buffer.

CA Characterization and SFE Analysis: CA of DNA functionalized interface was measured by using the DataPhysics' OCA25 system. For the measurements, a drop of 1 μL of ultrapure water was spotted on top of the gold substrate and the CA of drop was acquired after 10 s. The analysis was performed on a clean gold substrate, used as reference, and substrates functionalized with probes and probes–target biointerfaces. All contact angle values, measured in four replicas ($n = 4$), and relative standard deviations are collected in Figures S2–S5 of Supporting Information.

In parallel, the SFE was also evaluated by applying the OWRK model in CA. In this case, it was dosed 1 μL of ultrapure water and 1 μL of diiodomethane as reference values for the SFE calculation, reported in the wetting envelopes plots of Figure S6 (Supporting Information).

For the isoelectric properties analysis, the CA of 0.2 M phosphate buffer at pH 6.01, 0.2 M acetic acid/acetate buffers at pH 5.05, 4.01, acetate solution at pH 3.1 and hydrochloric acid 0.1 M at pH 2 drops were measured on step-by-step functionalized gold substrates. This acidic pH range, from 2 to 7, has been chosen to include the value of 5.5 at which the cooperative hybridization between LI probes and kDNA occurs.

EIS Measurements: EIS analysis was performed by using a PalmSens4 potentiostat (PalmSens, Netherlands) and assembling an electrochemical cell composed of Au electrode (CHI101) prepared according to the protocol described in Figure S7 (Supporting Information) as the working electrode (WE), a Pt wire as the counter electrode (CE), and an Ag/AgCl (KCl saturated) electrode used as reference electrode (RE). A solution of potassium hexacyanoferrate(III) ($K_3[Fe(CN)_6]$) 5×10^{-3} M diluted in PBS 10×10^{-3} M at pH 5.5 was employed as redox mediator. To verify the probes anchoring to the Au surface, EIS analysis was done in the frequency range of 0.1 Hz to 100 kHz while current and potential were fixed at 1 mA and open circuit potential (0.230 V), respectively. For the data fitting, an equivalent circuit system has been used, where R1 represents the electrical resistance of the electrolyte, C1 the double-layer capacitance at the WE–electrolyte interface, and R2 the charge transfer resistance due to the redox reaction of $[Fe(CN)_6]^{3-/4-}$ with the WE. Finally, W1 describes the Warburg impedance due to the diffusion process of reactants.

Computational Details: The theoretical study has been performed on the following platforms: 1) pure gold electrode (Au); 2) hydroxylated gold electrode (Au-OH); (3) probes-functionalized electrode (Au-probes). All platforms contained a single gold slab (111) (38 × 38 consisting of 1444 metal atoms) with a lattice constant of 4.08 Å.[49] The systems were energy-minimized by means CPMD software[50] that allows extending the calculations within plane wave approaches including periodic boundary conditions (PBC), precisely all the computational runs were carried out by the density functional theory (DFT) formalism using pseudopotentials (Goedecker-Teter-Hutter) to model the ionic potentials (Au_GTH_PBE.psp). The gradient corrected generalized gradient approximation (GGA) functional proposed by Perdew-Burke-Ernzerhof (PBE) was adopted.[51] The tolerances of energy, gradient, and displacement convergence were 2×10^{-5} Ha, 4×10^{-3} Ha Å^{-1}, and 5×10^{-3} Å, respectively. The kinetic energy cutoff for the planewaves was 50Ry, and the Gaussian smearing was used with a value of 0.2 eV for Brillouin-zone integration

in metals. Hence, the dipole correction was applied along the surface normal direction (z-direction). A planar water wafer of 500 molecules of H_2O was chosen for the simulation of the wet systems. The hydroxylated-metal slab was created by installing homogeneously hydroxyl groups all along the layer. The isolated ssDNA oligonucleotide probes were preliminary optimized using the hybrid exchange-correlation functional CAM-B3LYP[52] and the Pople basis set (6-311G(d,p)) was adopted as it proved to be quite valid in modelling the second-period elements.[53,54] The solvation environment was treated by using the integral equation formalism for the polarizable continuum model (IEF-PCM), the default parameters of Gaussian16[55] were used for the construction of the cavity, built as the envelope of interlocked spheres centered on each atom of the solute (water: $\epsilon = 78.3553$). Finally, Au-probes complex was generated by fixing LI1 and LI2 oligonucleotide strands equidistantly on the gold surface.

Supporting Information

Supporting Information is available from the Wiley Online Library or from the author.

Acknowledgements

This work was funded by the European Union's Horizon Europe EIC Pathfinder Open programme "ECLIPSE project" (Grant Agreement Nr. 101046787) and the European Union – FSE-REACT-EU, PON Research and Innovation 2014–2020 DM1062 / 2021 (CUP J45F21001750007).

Conflict of Interest

The authors declare no conflict of interest.

Author Contributions

P.C. and G.B. contributed equally to this work. The manuscript was written through contributions of all authors. All authors have given approval to the final version of the manuscript.

Data Availability Statement

The data that support the findings of this study are available from the corresponding author upon reasonable request.

Keywords

contact angle characterization, DNA–gold biointerface, *Leishmania infantum*, PCR-free detection, surface-free energy analysis

Received: August 2, 2024
Revised: October 1, 2024
Published online:

[1] S. Petralia, E. L. Sciuto, M. L. D. Pietro, M. Zimbone, M. G. Grimaldi, S. Conoci, *Analyst* **2017**, *142*, 2090.
[2] P. Nikolaou, E. L. Sciuto, A. Zanut, S. Petralia, G. Valenti, F. Paolucci, L. Prodi, S. Conoci, *Biosens. Bioelectron.* **2022**, *209*, 114165.
[3] A. A. Leonardi, E. L. Sciuto, M. J. Lo Faro, D. Morganti, A. Midiri, C. Spinella, S. Conoci, A. Irrera, B. Fazio, *Nanomaterials* **2022**, *12*, 2134.
[4] A. A. Leonardi, E. L. Sciuto, M. J. Lo Faro, B. Fazio, M. G. Rizzo, G. Calabrese, L. Francioso, R. Picca, F. Nastasi, G. Mancuso, C. Spinella, W. Knoll, A. Irrera, S. Conoci, *Nano Sel.* **2023**, *4*, 160.
[5] A. A. Leonardi, M. J. Lo Faro, S. Petralia, B. Fazio, P. Musumeci, S. Conoci, A. Irrera, F. Priolo, *ACS Sens.* **2018**, *3*, 1690.
[6] P. Calorenni, A. A. Leonardi, E. L. Sciuto, M. G. Rizzo, M. J. L. Faro, B. Fazio, A. Irrera, S. Conoci, *Adv. Healthcare Mater.* **2023**, *12*, 2300512.
[7] E. L. Sciuto, A. A. Leonardi, G. Calabrese, G. D. Luca, M. A. Coniglio, A. Irrera, S. Conoci, *Biomolecules* **2021**, *11*, 1585.
[8] M. Favetta, A. Valletta, G. Fortunato, M. E. Castagna, S. Conoci, E. L. Sciuto, T. Cosentino, F. Sinatra, S. Libertino, *Sens. Bio-Sens. Res.* **2015**, *6*, 72.
[9] D. Y. Zhang, *J. Am. Chem. Soc.* **2011**, *133*, 1077.
[10] A. W. Peterson, R. J. Heaton, R. M. Georgiadis, *Nucleic Acids Res.* **2001**, *29*, 5163.
[11] D. C. Rau, B. Lee, V. A. Parsegian, *Proc. Natl. Acad. Sci. USA* **1984**, *81*, 2621.
[12] R. Podgornik, D. C. Rau, V. A. Parsegian, *Macromolecules* **1989**, *22*, 1780.
[13] P. Gong, R. Levicky, *Proc. Natl. Acad. Sci. USA* **2008**, *105*, 5301.
[14] H. M. Watkins, A. J. Simon, F. Ricci, K. W. Plaxco, *J. Am. Chem. Soc.* **2014**, *136*, 8923.
[15] D. Bracha, E. Karzbrun, G. Shemer, P. A. Pincus, R. H. Bar-Ziv, *Proc. Natl. Acad. Sci. USA* **2013**, *110*, 4534.
[16] A. Johnson-Buck, J. Nangreave, S. Jiang, H. Yan, N. G. Walter, *Nano Lett.* **2013**, *13*, 2754.
[17] J. C. Traeger, Z. Lamberty, D. K. Schwartz, *ACS Nano* **2019**, *13*, 7850.
[18] J. Kiraga, P. Mackiewicz, D. Mackiewicz, M. Kowalczuk, P. Biecek, N. Polak, K. Smolarczyk, M. R. Dudek, S. Cebrat, *BMC Genomics* **2007**, *8*, 163.
[19] G. V. Sherbet, M. S. Lakshmi, *Biochim. Biophys. Acta, Biomembr.* **1973**, *298*, 50.
[20] G. V. Sherbet, M. S. Lakshmi, K. V. Rao, *Exp. Cell Res.* **1972**, *70*, 113.
[21] G. V. Sherbet, M. S. Lakshmi, F. Cajone, *Biophys. Struct. Mech.* **1983**, *10*, 121.
[22] P. Makkar, N. N. Ghosh, *RSC Adv.* **2021**, *11*, 27897
[23] N. Mardirossian, M. Head-Gordon, *Mol. Phys.* **2017**, *115*, 2315.
[24] G. Bella, A. Santoro, F. Nicolò, G. Bruno, M. Cordaro, *ChemPhysChem* **2021**, *22*, 593.
[25] A. Groß, S. Sakong, *Chem. Rev.* **2022**, *122*, 10746
[26] D. Zhao, F. Liu, X.-M. Duan, D.-Y. Sun, *Comput. Mater. Sci.* **2021**, *196*, 110533.
[27] Leishmania infantum: Trends in Parasitology https://www.cell.com/trends/parasitology/abstract/S1471-4922(19)30248-X?_returnURL=https%3A%2F%2Flinkinghub.elsevier.com%2Fretrieve%2Fpii%2FS147149221930248X%3Fshowall%3Dtrue. (accessed: July 2024).
[28] E. Camacho, A. Rastrojo, Á. Sanchiz, S. González-de la Fuente, B. Aguado, J. M. Requena, *Genes* **2019**, *10*, 758.
[29] I. Gow, N. C. Smith, D. Stark, J. Ellis, *Parasites Vectors* **2022**, *15*, 412.
[30] S. Petralia, S. Conoci, *ACS Sens.* **2017**, *2*, 876.
[31] R. A. Salathiel, *J. Pet. Technol.* **1973**, *25*, 1216.
[32] T. Tanaka, J. Lee, P. R. Scheller, in *Treatise on Process Metallurgy* (Ed: S. Seetharaman), Elsevier, Boston **2014**, pp. 61–77.
[33] Y.-N. Zhou, J.-J. Li, Z.-H. Luo, *AIChE J.* **2016**, *62*, 1758.
[34] S. Petralia, G. Forte, M. Zimbone, S. Conoci, *Colloids Surf., B* **2020**, *187*, 110648.
[35] P. Bergese, G. Oliviero, I. Colombo, L. E. Depero, *Langmuir* **2009**, *25*, 4271.
[36] F. Xia, Y. Zhu, L. Feng, L. Jiang, *Soft Matter* **2009**, *5*, 275.
[37] E. Virga, E. Spruijt, W. M. de Vos, P. M. Biesheuvel, *Langmuir* **2018**, *34*, 15174.
[38] I. M. Haune, A. Deblais, J. K. Beattie, H. Kellay, D. Bonn, *J. Phys. Chem. Lett.* **2017**, *8*, 1599.

[39] M. Kosmulski, *J. Colloid Interface Sci.* **2009**, *337*, 439.
[40] M. Gebala, W. Schuhmann, *ChemPhysChem* **2010**, *11*, 2887.
[41] A. T. Celebi, M. Olgiati, F. Altmann, M. Kogler, L. Kalchgruber, J. Appenroth, U. Ramach, M. Valtiner, L. L. E. Mears, in *Encyclopedia of Solid-Liquid Interfaces*, 1st ed. (Eds: K. Wandelt, G. Bussetti), Elsevier, Oxford **2024**, pp. 8–28.
[42] E. L. Sciuto, S. Petralia, G. Calabrese, S. Conoci, *Biotechnol. Bioeng.* **2020**, *117*, 1554.
[43] D. P. Chandler, L. Bryant, S. B. Griesemer, R. Gu, C. Knickerbocker, A. Kukhtin, J. Parker, C. Zimmerman, K. S. George, C. G. Cooney, *Microarrays* **2012**, *1*, 107.
[44] S. Petralia, R. Verardo, E. Klaric, S. Cavallaro, E. Alessi, C. Schneider, *Sens. Actuators, B* **2013**, *187*, 99.
[45] B. Foglieni, A. Brisci, F. S. Biagio, P. D. Pietro, S. Petralia, S. Conoci, M. Ferrari, L. Cremonesi, *Clin. Chem. Lab. Med.* **2010**, *48*, 329.
[46] C. Mary, F. Faraut, L. Lascombe, H. Dumon, *J. Clin. Microbiol.* **2004**, *42*, 5249.
[47] J. L. Weirather, S. M. B. Jeronimo, S. Gautam, S. Sundar, M. Kang, M. A. Kurtz, R. Haque, A. Schriefer, S. Talhari, E. M. Carvalho, J. E. Donelson, M. E. Wilson, *J. Clin. Microbiol.* **2011**, *49*, 3892.
[48] A. M. D. Pascali, R. Todeschini, S. Baiocchi, M. Ortalli, L. Attard, A. V. Ibarra-Meneses, E. Carrillo, S. Varani, *PLoS Neglected Trop. Dis.* **2022**, *16*, e0010676.
[49] W.-K. Li, G.-D. Zhou, T. Mak, W.-K. Li, G.-D. Zhou, T. Mak, *Advanced Structural Inorganic Chemistry*, Oxford University Press, Oxford **2008**.
[50] Car-Parrinello Molecular Dynamics, https://github.com/CPMD-code (accessed: March 2024).
[51] J. P. Perdew, K. Burke, M. Ernzerhof, *Phys. Rev. Lett.* **1996**, *77*, 3865.
[52] T. Yanai, D. P. Tew, N. C. Handy, *Chem. Phys. Lett.* **2004**, *393*, 51.
[53] B. Ferrari, C. Bennett, *J. Phys.: Conf. Ser.* **2019**, *1290*, 012013.
[54] G. Bella, A. Santoro, M. Cordaro, F. Nicolò, G. Bruno, *Chin. J. Chem.* **2020**, *38*, 163.
[55] M. J. Frisch, G. W. Trucks, H. B. Schlegel, G. E. Scuseria, M. A. Robb, J. R. Cheeseman, G. Scalmani, V. Barone, G. A. Petersson, H. Nakatsuji, X. Li, M. Caricato, A. V. Marenich, J. Bloino, B. G. Janesko, R. Gomperts, B. Mennucci, H. P. Hratchian, J. V. Ortiz, A. F. Izmaylov, J. L. Sonnenberg, D. Williams-Young, F. Ding, F. Lipparini, F. Egidi, J. Goings, B. Peng, A. Petrone, T. Henderson, D. Ranasinghe, et al., Gaussian, Inc., Wallingford CT, **2016**. Website: https://gaussian.com (accessed: March 2024).